Electronic Supplementary Information

Immobilization of catalytic sites on quantum dots by ligand bridging for photocatalytic CO_2 reduction

Yipeng Bao,[a] Jin Wang,*[a] Qi Wang,[a] Xiaofeng Cui,[c] Ran Long,[b] and Zhengquan Li*[a]

[a] *Key Laboratory of the Ministry of Education for Advanced Catalysis Materials, Zhejiang Normal University, Jinhua, Zhejiang 321004, P. R. China. E-mail: wangjin@zjnu.edu.cn; zqli@zjnu.edu.cn*

[b] *Hefei National Laboratory for Physical Sciences at the Microscale, iChEM (Collaborative Innovation Center of Chemistry for Energy Materials), School of Chemistry and Materials Science, and National Synchrotron Radiation Laboratory, University of Science and Technology of China, Hefei, Anhui 230026, P. R. China*

[c] *Anhui Key Laboratory of Photoelectric-Magnetic Functional Materials, School of Chemistry and Chemical Engineering, Anqing Normal University, Anqing, Anhui 246011, P. R. China*

1. Sample Characterizations:

Prior to electron microscopy characterizations, a drop of the suspension of particles (H_2O and alcohol, 1:3) was placed on a piece of carbon-coated copper grid and dried under ambient conditions. Transmission electron microscopy (TEM) image were taken on a JEOL JEM-2100F field-emission high-resolution transmission electron microscope operated at 200 kV.

Powder XRD patterns were recorded by using a Philips X'Pert Pro Super X-ray diffractometer with Cu-Kα radiation (λ =1.5418Å).

UV-vis absorption spectra were recorded on a Shimadzu 2501PC UV-vis spectrophotometer.

^{1}H NMR spectra were acquired on a 600 MHz Bruker Avance III with a 5 mm TXI probe using TopSpin 3.1. MestReNova was used to plot NMR spectra.

Steady-state photoluminescence (PL) spectra were collected by a FluoroMax-4 spectrofluorometer (Horiba Scientific) and analyzed with an Origin-integrated software (FluoroEssencev2.2). The PL decay spectra were recorded on a photoluminescence spectrometer (FLS980, Edinburgh Instruments Ltd.) with a 380-nm excitation wavelength and a 565-nm emission wavelength with the time-correlated single-photon counting (TCSPC) mode. The lifetime data were analyzed with DataStation v6.6 (Horiba Scientific).

X-ray photoelectron spectroscopy (XPS) and Fe $L_{2,3}$-edge and S $L_{2,3}$-edge near edge X-ray absorption fine structure spectroscopy (NEXAFS) experiments were performed at the Photoemission Endstation (BL10B) in the National Synchrotron Radiation Laboratory (NSRL), Hefei, China.

The content of ligands in solution was determined on an Agilent 1260 Infinity II High-Performance Liquid Chromatography (HPLC). The reacted solution was mixed with an equal volume of ethanol precipitator, and then centrifuged to remove CdTe QDs. The mobile phase was ethanol:H_2O = 1:1 with a flow rate of 1.0 mL·min^{-1}.

Detection of Fe^{3+} ions: It is well known that the colorless Fe^{3+}(aq) and KSCN(aq) react to form a red product, $[Fe(SCN)]^{2+}$(aq). So the absorbance of the solution can be used to measure the amount of Fe^{3+} generated in the photocatalytic system. Therefore, we centrifuged the CdTe-b-$Fe_{(4)}$ containing excess iron ions, and added KSCN solution to the supernatant to detect the presence of Fe^{3+} ions (as shown in Fig. S10b).

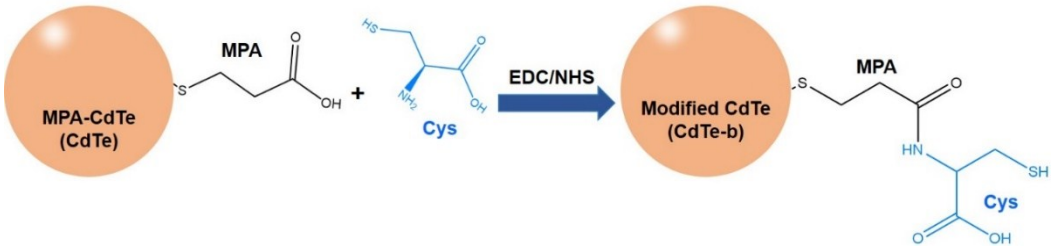

Fig. S1 Schematic illustration for the grafting process of Cys on the pristine MPA-capped CdTe QDs.

The MPA ligands were naturally capped on CdTe QDs with thiol groups during the synthesis, leaving free carboxylic groups pointing outward. These carboxylic groups can be employed to link amino groups of Cys by forming amide bonds. The CdTe QDs modified with Cys are denoted as CdTe-b.

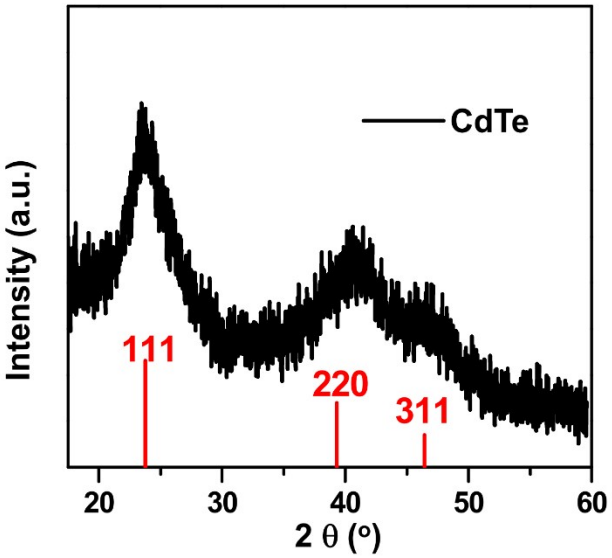

Fig. S2 Powder XRD patterns of CdTe QDs. The standard diffraction for CdTe (bulk cubic, JCPDS card no. 65-1046) is provided as a reference.

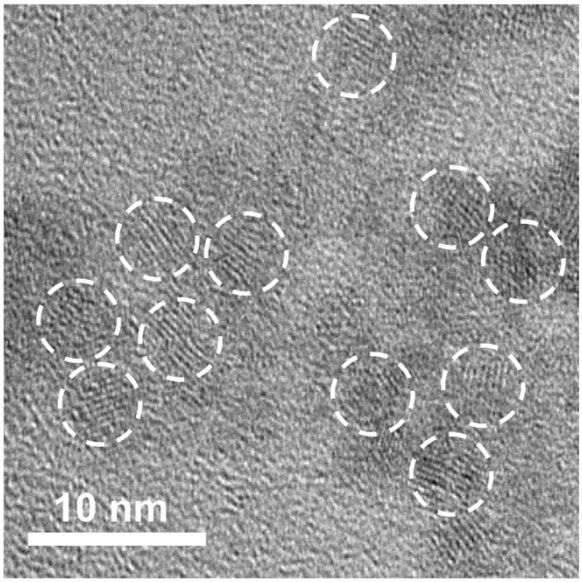

Fig. S3 TEM of the as-prepared CdTe QDs.

According to TEM, the as-prepared water-soluble CdTe QDs are uniformly distributed spherical nanoparticles with an average particle diameter of about 3.8 nm.

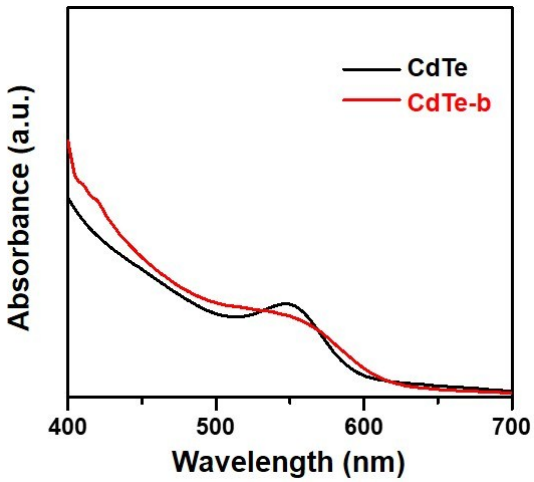

Fig. S4 UV-vis absorption spectra of CdTe and CdTe-b QDs in aqueous dispersion.

Fig. S4 shows the absorption spectra of CdTe QDs before and after ligand modification. Obviously, after the CdTe QDs were modified with cysteine ligands, the absorption peak positions of the CdTe QDs showed only a slight change, indicating that the ligand modification process did not significantly affect the inherent photoelectric properties of the CdTe QDs.

The concentration of QDs can be estimated by the following empirical equations:

$D = (9.8127\times10^{-7})\ \lambda^{□} - (1.7147\times10^{-3})\ \lambda^{□} + (1.0064)\ \lambda - 194.84$

$□ = 10043\ (D)^{2.12}$

$C = A/(\varepsilon L)$

where D (nm) is the size of a given nanocrystal, λ (nm) is the wavelength of the first excitonic absorption peak, A is the absorbance at the maximum of the first excitonic absorption peak, C is the molar concentration (mol/L) of nanocrystals, and L is the path length (cm) of the radiation beam used to collect the absorption spectrum.[1] Calculated by the equations, the concentration of the as-prepared CdTe QDs (Fig. S4) in our work is about 5.0 μM.

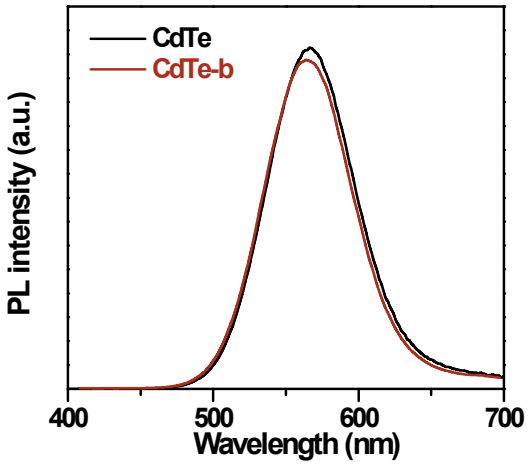

Fig. S5 PL spectra of CdTe and CdTe-b (modified) QDs in aqueous dispersion, respectively.

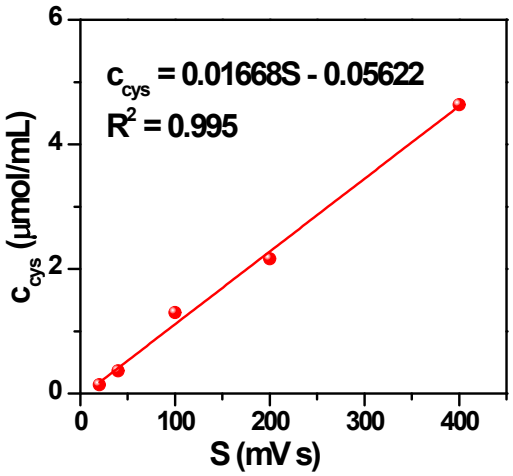

Fig. S6 Standard curve for the quantitative analysis of Cys concentration by HPLC.

To quantify the amount of Cys on per QD particle, we have managed to analyze the amount of Cys left in solution by HPLC after the grafting process and then calculated the Cys amount attached on QDs. Based on the standard curves in Fig. S6, it turns out that about 0.46 μmol of Cys has grafted to the 0.005 μmol MPA-CdTe QDs, the molar ratio of Cys to QDs is 92:1.

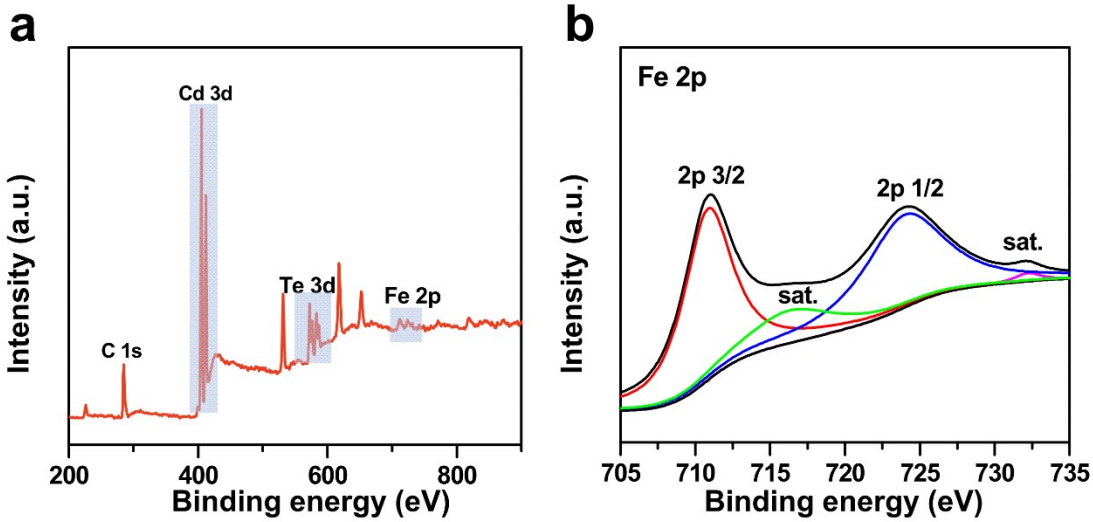

Fig. S7 (a) XPS survey spectrum of CdTe-b-Fe QDs. (b) High resolution Fe 2p XPS spectrum of CdTe-b-Fe QDs.

In order to study whether Fe^{2+} ions are effectively immobilized on the surface of CdTe-b-Fe QDs, we centrifuged the as-prepared CdTe-b-Fe QD samples and the precipitate was analyzed by XPS technique. In Fig. S7a, the XPS spectra showed strong Cd, Te signals and the relatively weak Fe signals, indicating the co-existence of CdTe and Fe. We further characterized the Fe in the sample by high-resolution XPS and found that the Fe contained in the CdTe-b-Fe QDs was divalent Fe^{2+} (Fig. S7b). As a comparison, the similar method was adopted to introduce Fe^{2+} ions into the unmodified CdTe QDs solution, and then centrifuged the QD samples. However, we did not observe the presence of iron in the precipitate. The above results demonstrate that this ligand bridging strategy can effectively immobilize Fe^{2+} on the surface of CdTe QDs.

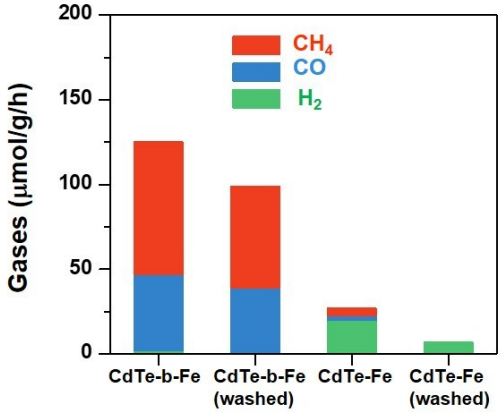

Fig. S8 Production rates of CH_4, CO and H_2 in light-driven CO_2 reduction with H_2O in the presence of TEOA, catalyzed by CdTe-b-Fe (Cys-modified) and pristine CdTe-Fe (MPA-CdTe with Fe^{2+} ions) before and after removing free Fe^{2+} from the solution.

To better clarify the advantage of Cys-modified CdTe QDs (CdTe-b), we have assessed the photocatalytic performance of pristine MPA-CdTe (1 μM, QD particles) and CdTe-b (1 μM, QD particles) immersed in Fe^{2+} solution (50 μM) before and after washing (Fig. S8). For the pristine MPA-CdTe QDs, due to the lack of metal catalytic sites (Fe^{2+}) after washing, the photocatalytic properties of QDs declines significantly. As for the Cys-modified CdTe QDs, there are thiol groups pointing outward on their surface, which can effective immobilize Fe^{2+} ions. After washing, most of the Fe^{2+} ions remain on the QD surface so that their catalytic activities do not decrease significantly. In the latter case, instead of trapping electrons by random collisions, the metal ions (e.g., Fe^{2+}) can capture photogenerated electrons from QDs through the ligands, thereby promoting the reduction of CO_2. The results further confirm that the Fe^{2+} ions can be immobilized to the surface of Cys-modified CdTe QDs and serve as active sites for photocatalytic CO_2 reduction.

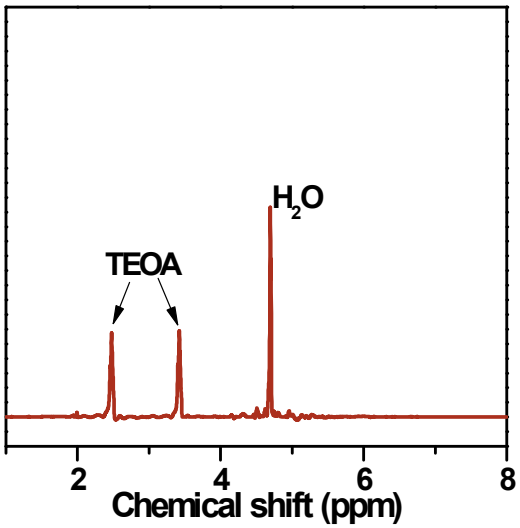

Fig. S9 ^{1}H-NMR spectra of the liquid phase taken from the reaction system after visible light irradiation for 2 h.

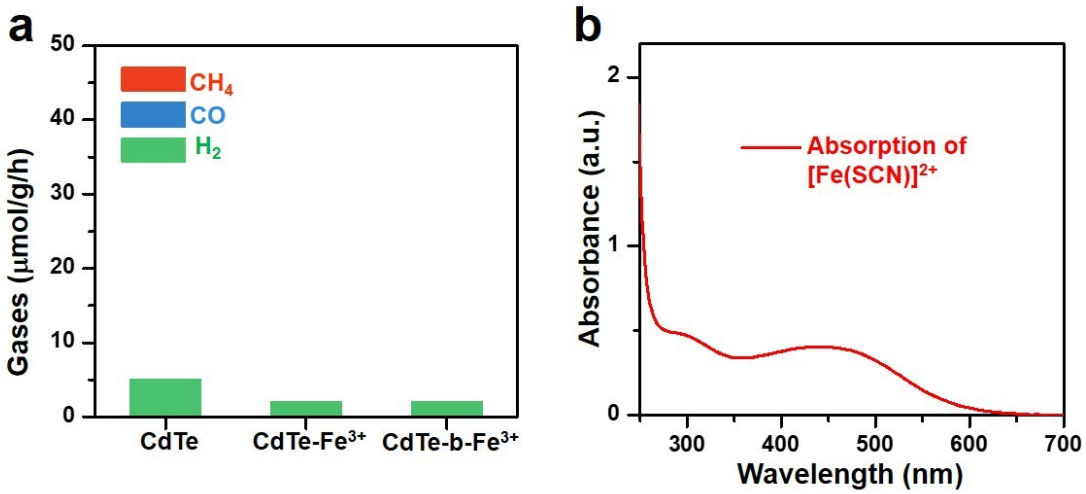

Fig. S10 (a) Photocatalytic performance of CdTe, CdTe-Fe^{3+} and CdTe-b-Fe^{3+}. (b) Detecting the presence of Fe^{3+} ions in CdTe-b-$Fe_{(4)}$: the absorption of the supernatant after adding KSCN (see details in sample characterizations).

We have mentioned that the presence of Fe^{3+} may affect the catalytic activities of our photocatalytic system. To investigate whether the Fe^{2+} ions are oxidized to Fe^{3+} ions and its effect on photocatalysis, we conducted some control experiments. As shown in Fig. S11a, when Fe^{3+} ions are directly added to CdTe QDs (CdTe-Fe^{3+}), these free ions reduce the catalytic activity of the QDs; when the Fe^{3+} ions are added to the CdTe-b QDs (CdTe-b-Fe^{3+}), these bridged ions also reduce the catalytic activity of the QDs. Taken together, the above experiments show that the presence of Fe^{3+} ions is not conducive to the catalytic reaction of the system. When an excessive amount of Fe^{2+} ions is added to the CdTe-b QDs (or CdTe QDs), some of the free Fe^{2+} iron ions can be easily oxidized to Fe^{3+} ions (as confirmed by Fig. S11b), resulting in a decrease in the overall catalytic activity of the CdTe-b-Fe QDs (or CdTe-Fe). This also indicates that the ligand bridging strategy is helpful in immobilizing the divalent Fe^{2+} ions to prevent them from being oxidized.

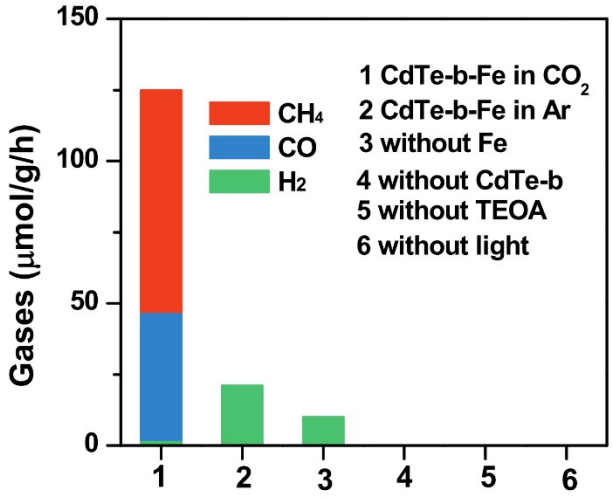

Fig. S11 Control photocatalytic experiments using CdTe-b-Fe QDs as catalysts under different conditions.

The control photocatalytic experiments show that the CdTe-b-Fe QDs can only reduce protons to H_2 in Ar atmosphere (**2**), which further confirms that the carbon-based reduction products in the CO_2 atmosphere are mainly derived from CO_2 instead of organic substances in system. Without the use of Fe^{2+} ions (**3**), only a small amount of H_2 is produced; in addition, in the absence of CdTe-b QDs (**4**) or sacrificial agents (**5**), or in the dark conditions (**6**), no obvious products were detected. The above results indicate that CdTe-b-Fe QDs are the photocatalysts, in which Fe^{2+} ions act as the catalytic centers and CdTe-b QDs serve as the photosensitizers.

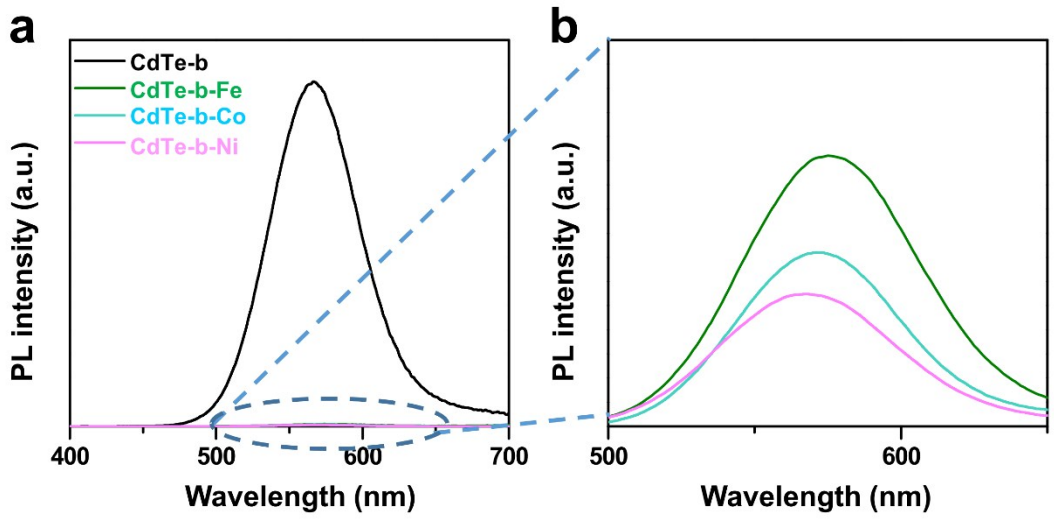

Fig. S12 PL emission curves of CdTe-b QDs bridged with different metal ions (λ_{ex}= 380 nm).

The steady-state PL emissions of CdTe-b QDs bridged with different ions (Fe^{2+}, Co^{2+} and Ni^{2+}) are shown in Fig. S12. In comparison with CdTe-b QDs, these PL emissions exhibit obvious quenching effect after bridging metal ions, showing that the radiative recombination were suppressed due to the fact that many photoexcited electrons have been transferred to the metal sites. Above results also implies that the ligand bridging strategy is valid for immobilizing other metal ions onto CdTe QDs.

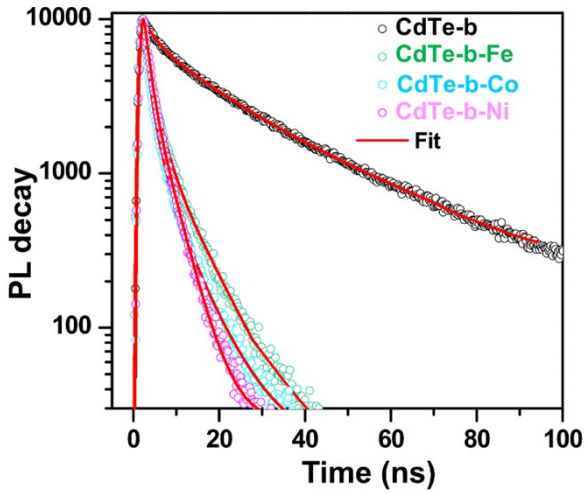

Fig. S13 Transient-state PL (TRPL) curves of CdTe-b QDs anchored with different metal ions (λ_{ex}= 380 nm, λ_{em}= 565 nm).

The lifetimes of samples (Fig. S13) can be fitted according to the bi- and tri-exponential decay kinetics, which can be calculated using the following expression:

$$\tau_{avg} = \frac{\sum_n (A_n \tau_n^2)}{\sum_n (A_n \tau_n)}$$

Where *n* corresponds to the n^{th} component of a given multiexponential decay process.[2]

Table S1 Fit parameters of PL decay curves CdTe-b QDs bridged with various metal ions.[a]

Samples	A_1	A_2	A_3	τ_1 (ns)	τ_2 (ns)	τ_3 (ns)	τ_{avg} (ns)	k_{et} (10^7 s^{-1})
CdTe-b	2809	8290		6.2	32.0		30.4	
CdTe-b-Fe	6708	765	26640	4.2	12.3	1.2	3.9	22.4
CdTe-b-Co	9760	760	87495	3.0	6.0	0.8	1.6	57.4
CdTe-b-Ni	8266	890	88834	2.5	5.8	0.7	1.4	66.9

[a]Determined using the fitting function $y = B + A_1 \exp(-t/\tau_1) + A_2 \exp(-t/\tau_2) + a_3$

$\exp(-t/\tau_3)$.

The transient PL decay of CdTe-b QDs bridged with different ions (Fe^{2+}, Co^{2+} and Ni^{2+}) are shown in Fig. S13. After bridging with above metal ions, the PL lifetimes of samples become shorter in comparison with CdTe-b QDs. The shortened lifetimes of QDs further confirm that many photoexcited electrons have been transferred to the metal ions, so that the radiative electron-hole recombination is suppressed. Moreover, with the bridging of Fe^{2+}, Co^{2+} or Ni^{2+} ions, the lifetime of CdTe-b QDs is gradually decreased from 3.9 ns to 1.4 ns, and the electron transfer rate is gradually increased from 22.4×10^7 to 66.9×10^7 s^{-1}. A higher electron injection rate means that more photoexcited electrons will be able to be captured by metal ions for photocatalytic reactions. This can also explain in part why the overall catalytic activity of CdTe-b-Co (Ni) QDs is higher than that of CdTe-b-Fe QDs in Fig. 7.

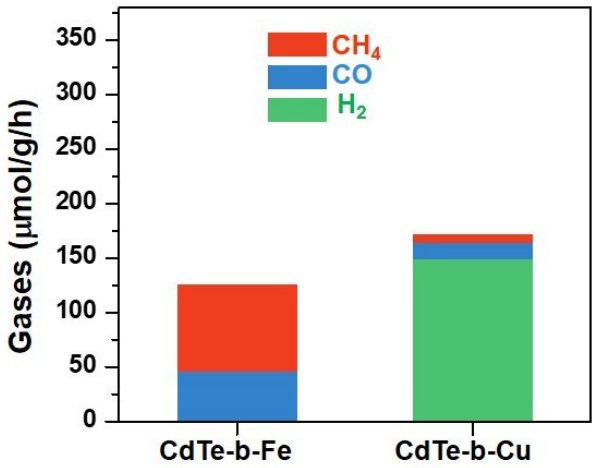

Fig. 14 Production rates of CH_4, CO, and H_2 by CdTe-b QDs based catalysts bridged with Fe^{2+} and Cu^{2+} cations.

A big merit of our strategy is the versatility of metal ions that can be readily bridged onto CdTe QDs, which allows correlating the catalytic performance with different metal ions. Fig. S14 shows the average gas production rates of CH_4, CO, and H_2 by CdTe-b grafted with Cu^{2+} cations. Apparently, the Cu^{2+} ions are favorable to produce H_2 from H_2O, rather than CO or CH_4 from CO_2, and the overall catalytic performance for CO_2 reduction is lower than Fe^{2+} ions. This result may probably due to the different electronic structures between Cu^{2+} and other metal cations.[3]

Reference

1. W. W. Yu, L. Qu, W. Guo, X. Peng, *Chem. Mater.* 2003, **15**, 2854-2860.
2. D. R. James, Y.-S. Liu, P. De Mayo, W. R. Ware, *Chem. Phys. Lett*. 1985, **120**, 460-465.
3. X. F. Cui, J. Wang, B. Liu, S. Ling, R. Long, Y. J. Xiong, *J. Am. Chem. Soc.* 2018, **140**, 16514-16520.